Frontiers of Information Technology & Electronic Engineering
www.jzus.zju.edu.cn; engineering.cae.cn; www.springerlink.com
ISSN 2095-9184 (print); ISSN 2095-9230 (online)
E-mail: jzus@zju.edu.cn

Generation of noise-like pulses and soliton rains in a graphene mode-locked erbium-doped fiber ring laser*

Pinghua TANG[1], Mulin LUO[1], Ting ZHAO‡[2], Yuliang MAO‡[1]

[1]*Hunan Key Laboratory for Micro-Nano Energy Materials and Devices, School of Physics and Optoelectronics, Xiangtan University, Xiangtan 411105, China*

[2]*School of Electronic Engineering, Nanjing Xiaozhuang University, Nanjing 211171, China*

E-mail: pinghuatang@xtu.edu.cn; 1011773923@qq.com; zthaza@126.com; ylmao@xtu.edu.cn

Received July 24, 2020; Revision accepted Nov. 25, 2020; Crosschecked Jan. 18, 2021; Published online Jan. 30, 2021

Abstract: We demonstrate the generation of noise-like pulses (NLPs) and soliton rains in a graphene saturable absorber mode-locked erbium-doped fiber laser. Typical NLPs are obtained at a proper pump power and in a cavity polarization state. The soliton rain operation with multiple solitons can be achieved by finely adjusting the cavity polarization state. In addition, distinctive multi-soliton interactions are observed and investigated, including the fundamental mode-locking and multiple pulses. The experimental results can help further understand nonlinear pulse dynamics in ultrafast optics.

Key words: Erbium-doped fiber lasers; Graphene; Saturable absorption; Passive mode-locking
https://doi.org/10.1631/FITEE.2000372 **CLC number:** TN248

1 Introduction

Over the past decade, passively mode-locked fiber lasers (MLFLs) have been extensively investigated, and there have been remarkable advances in scientific and industrial applications. Different from active mode-locked techniques, the passive mode-locked scheme is simple, compact, and low cost, without using complex and costly active modulators and drivers in the laser cavity. Typically, passively MLFLs can be implemented based on nonlinear polarization rotation (NPR) (Chouli and Grelu, 2010; Jeong et al., 2014; Liu et al., 2015; Ma R et al., 2019), nonlinear amplifying loop mirror (NALM) (Niang et al., 2014; Ning et al., 2014; Luo AP et al., 2015), semiconductor saturable absorber mirror (SESAM) (Tang PH et al., 2015), novel two-dimensional material saturable absorbers (SAs) like graphene and graphene oxide (Bao et al., 2009; Ng et al., 2020), topological insulator (Zhao et al., 2012; Luo ZC et al., 2013), transition metal sulfide (Zhang et al., 2014; Woodward et al., 2015), black phosphorus (Ahmed et al., 2016; Song et al., 2016), MXene (Li J et al., 2019; Ma CY et al., 2020), and tellurium (Shi et al., 2020). Among them, graphene is now believed to be a promising SA, and has been widely used in mode-locking (Zhang et al., 2009; Martinez et al., 2010; Meng et al., 2012; Song et al., 2013; Popa et al., 2017; Yun, 2017; Pawliszewska et al., 2018) and Q-switching (Popa et al., 2011; Tang YL et al., 2014; Ahmad et al., 2017; Li D et al., 2017; Kasim et al., 2018; Liu J et al., 2021) because of its excellent

‡ Corresponding authors

* Project supported by the Hunan Provincial Natural Science Foundation of China (Nos. 2018JJ3514 and 2019JJ40280), the Research and Development Plan of Key Areas in Hunan Province in 2019 (No. 2019GK2101), the Jiangsu Provincial Natural Science Foundation of China (No. BK20181050), the Natural Science Foundation of Jiangsu Higher Education Institutions of China (Nos. 18KJB413007 and 19KJB10061), and the 2019 Youth Special Scientific Research Project of Nanjing Xiaozhuang University, China (No. 2019NXY17)

ORCID: Pinghua TANG, https://orcid.org/0000-0003-2285-9812; Ting ZHAO, https://orcid.org/0000-0002-7695-9133; Yuliang MAO, https://orcid.org/0000-0003-1391-914X

saturable absorption effect.

As one kind of special soliton state, noise-like pulses (NLPs) can be frequently observed in the passively mode-locked erbium-doped fiber lasers (EDFLs), and are characterized by a broad pulse with a smooth and wide spectrum as well as an autocorrelation trace featuring a narrow peak on a broad pedestal (Wang et al., 2016). Because of their unique features such as high pulse energy, wide optical bandwidth, and low coherence, NLPs are attractive for several important applications including supercontinuum generation (Zaytsev et al., 2013), nonlinear frequency conversion (Kobtsev et al., 2014; Smirnov et al., 2014), sensing (Goloborodko et al., 2003), and micromachining (Ozgören et al., 2011). Systematic investigation on NLPs in NPR based mode-locked EDFLs (Jeong et al., 2014; Liu J et al., 2015) and figure-eight fiber lasers (Niang et al., 2014; Ning et al., 2014) has been carried out. In addition to NLPs, the soliton rain phenomenon can be observed in passively MLFLs. This occurs in the transition region between the conventional soliton pulse and continuous-wave operation state (Chouli and Grelu, 2010). The pulse state of soliton rains is composed of two parts, the soliton flow part and the soliton condensed part, where solitons are constantly moving from the flow part to the condensed part. This is similar to the process of rain droplet formation in nature (Song et al., 2013). Although NLP and soliton rain phenomena have been observed in the passively MLFLs by many researchers, switchable operation regimes between them in the same laser cavity, especially in the two-dimensional materials based mode-locked EDFLs, have been rarely reported. Clearly, compared to the single operation state, lasers that can switch between NLPs and soliton rains have more advantages. Moreover, it would be beneficial for understanding nonlinear pulse dynamics in ultrafast optics to systematically investigate this switching process.

Here, we study the experimental observation of the dynamic generation processes of soliton NLPs and soliton rains in a graphene mode-locked EDFL. By adjusting the polarization controller (PC), we observe the switching between NLPs and soliton rains. Investigation on the transition between soliton rains and other pulse states can promote the understanding of the complex soliton dynamics in passively mode-locked EDFLs.

2 Fabrication and nonlinear optical characterization of a graphene saturable absorber

The structure of the graphene saturable absorber (GSA) is depicted in the insert of Fig. 1, where a tapered fiber with the tapered area covered by graphene (5 mm×5 mm) is sandwiched by an MgF_2 substrate and a polydimethylsiloxane (PDMS). The tapered fiber with a diameter of 6 μm and a length of 5 mm is drawn from a standard single-mode fiber (SMF) by flame-brushing technology. The MgF_2 and PDMS have a refractive index of 1.376 and 1.413, respectively. The small refractive index discrepancy between the MgF_2 and PDMS means that they would have a small effect on the evanescent field of the tapered fiber.

After successful fabrication of the GSA, we focus on the characterization of its polarization-dependent saturable absorption via a balanced twin-detector measurement technique (Tang PH et al., 2016). The experimental measurement configuration is schematically shown in Fig. 1. A home-made pulsed laser (central wavelength of 1560 nm, pulse duration of 1 ps, and repetition rate of 21 MHz) amplified by an erbium-doped fiber amplifier (EDFA) functions as the light source. A PC and a fiber polarizer are used to produce the linearly polarized incident light with a tunable polarization state.

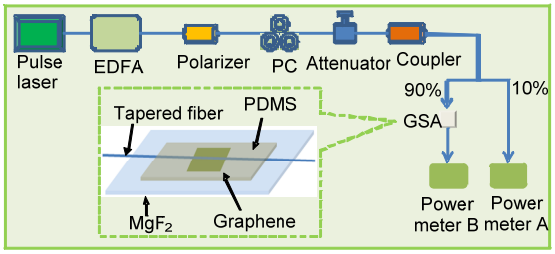

Fig. 1 Measurement of polarization-dependent absorption of the graphene saturable absorber (GSA)
Insert is the structure of the tapered fiber based GSA. EDFA: erbium-doped fiber amplifier; PC: polarization controller; PDMS: polydimethylsiloxane

Fig. 2 shows the measured nonlinear absorption curves of the GSA for TE and TM modes. When the incident light power increases from 1 to 30 mW, the transmittance of the GSA for the TE mode increases from 5.6% to 10.6%. For the TM mode, the transmittance increases from 0.11% to 0.81%. The corresponding modulation depth is about 5% and

0.7% for TE and TM modes, respectively. These results indicate that both the insertion loss (IL) and polarization-dependent loss (PDL) are extremely large. We investigate IL and PDL using the KEYSIGHT equipment (8184B, N7786B, N7744A, Keysight, USA). Results are shown in Fig. 3. As shown in Fig. 3a, IL is larger than 12 dB from 1500 to 1600 nm. Fig. 3b indicates that PDL is also large, larger than 10 dB, which basically agrees with the transmittance values of the two orthogonal modes depicted in Fig. 2. The large PDL can be attributed to the different interaction magnitudes for the TE and TM modes with the tapered-fiber/graphene. In this GSA structure, the electric field of TE mode is parallel to the graphene film. This means that they suffer from a lower propagation loss than for the TM mode (Sheng et al., 2013). The large PDL means that GSA can be considered as a polarizer.

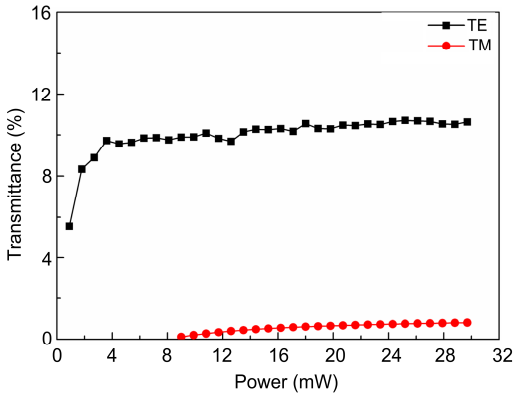

Fig. 2 Nonlinear absorption of the graphene saturable absorber for TE and TM modes

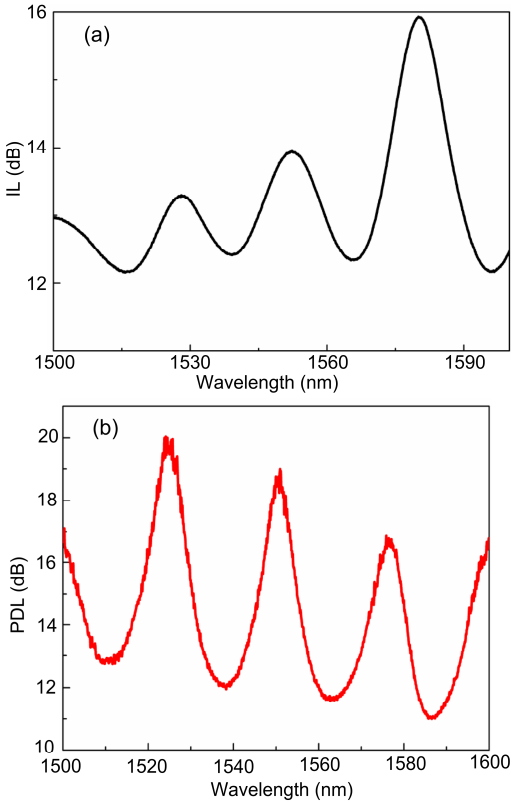

Fig. 3 Insertion loss (IL) (a) and polarization-dependent loss (PDL) (b) of the graphene saturable absorber

3 Experimental setup

The experimental setup of the passively mode-locked EDFL based on the GSA is shown in Fig. 4. A length of 8 m erbium-doped fiber (EDF) (EDFC-980-HP, Nufern, USA) is pumped by a 980-nm laser diode (LD) through a fused wavelength division multiplexer (WDM). The EDF used in the experiment has an absorption coefficient of (6±1) dB/m at 1530 nm and a group velocity dispersion (GVD) of 15.5 ps^2/km at 1550 nm. SMFs are used as the dispersion compensation components with a GVD of −23 ps^2/km at 1550 nm. A PC is used to adjust the cavity polarization state, and a polarization-independent isolator (PI-ISO) is used to ensure the unidirectional transmission in the ring cavity. The laser output is directed through the 10% port of a coupler. The total cavity length is 28.6 m, and the net dispersion of the cavity is −0.35 ps^2. The output spectra are measured by an optical spectrum analyzer (AQ6370C, Yokogawa, Japan). The autocorrelation trace is monitored by an

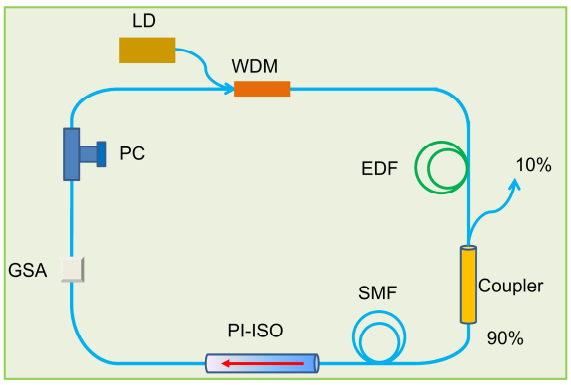

Fig. 4 Experimental setup of the GSA mode-locked erbium-doped fiber laser

PC: polarization controller; WDM: wavelength division multiplexer; EDF: erbium-doped fiber; SMF: single-mode fiber; GSA: graphene saturable absorber; LD: laser diode; PI-ISO: polarization-independent isolator

autocorrelator (FR-103XL, Femtochrome, USA). The output pulse train is detected by a 1-GHz, 5-GS/s oscilloscope (DL9140, Yokogawa, Japan) together with a 1.2-GHz bandwidth photodetector (DET01CFC, Thorlabs, USA).

4 Results and discussion

4.1 Noise-like pulses

When the pump power is set to 57 mW, we obtain the NLP mode-locked state by adjusting the PC appropriately. Results are shown in Fig. 5. As shown in Fig. 5a, there are two peaks in the output spectrum, with the center wavelengths locating at 1531 nm and 1557 nm. The front peak at 1531 nm with a relatively weak intensity is induced by a large IL (Zeng et al., 2015). Fig. 5b shows the mode-locked pulse train, from which we can see that the fundamental repetition frequency is about 7 MHz, which corresponds to the total cavity length of the laser. The output power is about 1.4 mW.

The autocorrelation trace of NLPs is shown in Figs. 5c and 5d, exhibiting a narrow coherent peak with a full width at half-maximum (FWHM) duration of 650 fs on a broad pedestal of 90 ps. The unique characteristics of the autocorrelation trace together with the broad and smooth optical spectrum indicate that the mode-locked pulses obtained are NLPs, as reported in Jeong et al. (2014) and Liu et al. (2015). In addition, the operational state of NLPs can be maintained when the pump power changes from 57 to 520 mW by appropriately adjusting the PC. It should be noted that the PC is slightly adjusted to optimize the cavity polarization by changing the cavity birefringence. The formation of the mode-locked NLPs in our experiment may be greatly related to the cavity polarization state as the PDL of the GSA exceeds 10 dB from 1500 to 1600 nm.

4.2 Soliton rains

Another distinct mode-locked state with multiple solitons is observed by properly adjusting the PC under the pump power of 57 mW. This state is known

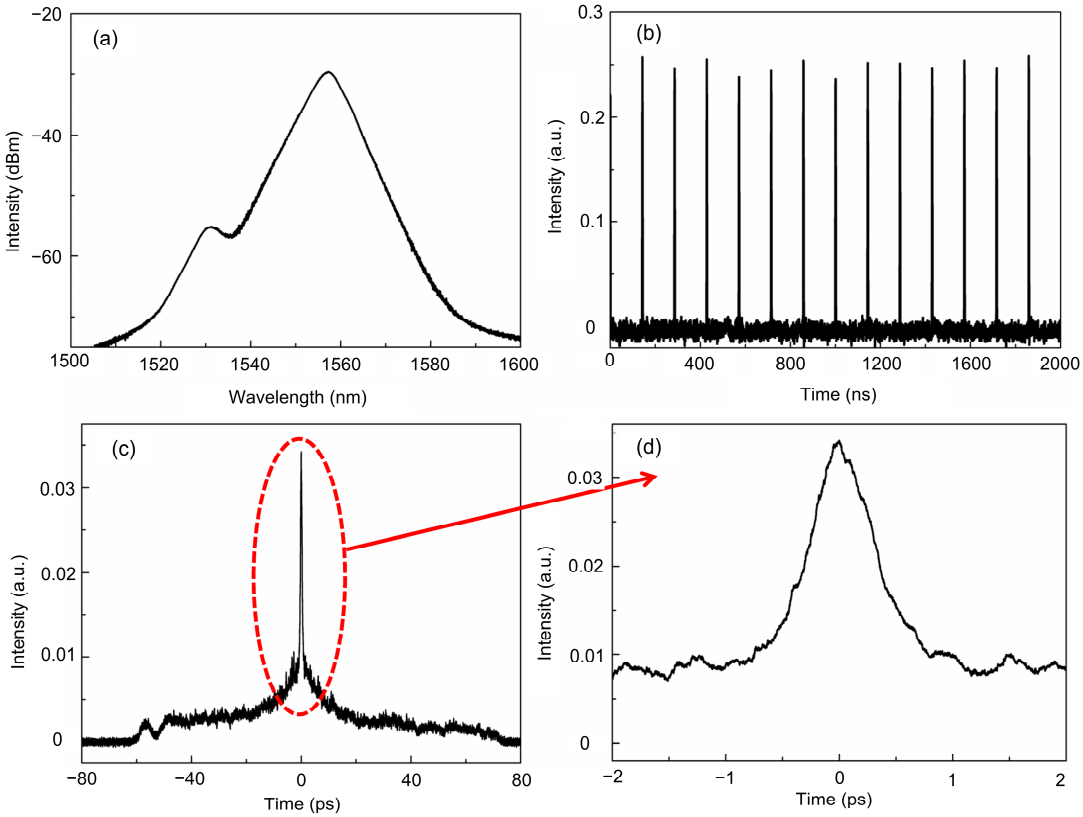

Fig. 5 Characteristics of the graphene saturable absorber mode-locked erbium-doped fiber laser operating in a noise-like pulse state: (a) optical spectrum; (b) output pulse train; (c) autocorrelation trace; (d) magnified autocorrelation trace in (c)

as the soliton rain state (Chouli and Grelu, 2010). Fig. 6a shows a typical temporal profile of the soliton rain state on the oscilloscope. The temporal separation between adjacent pulse bunches is about 143 ns, corresponding to the roundtrip time of the laser cavity. It can be seen from Fig. 6b that several independent solitons are preceding the main pulse, and that their energy distribution is uneven, comprising only a small proportion of the total energy of the pulse bunch. As can be seen from Fig. 6c, there are obvious quasi continuous wave (CW) spectral components around 1530 nm, and Kelly sidebands exist. This shows that the mode-locked fiber laser is operated in the anomalous dispersion regime (Nelson et al., 1997).

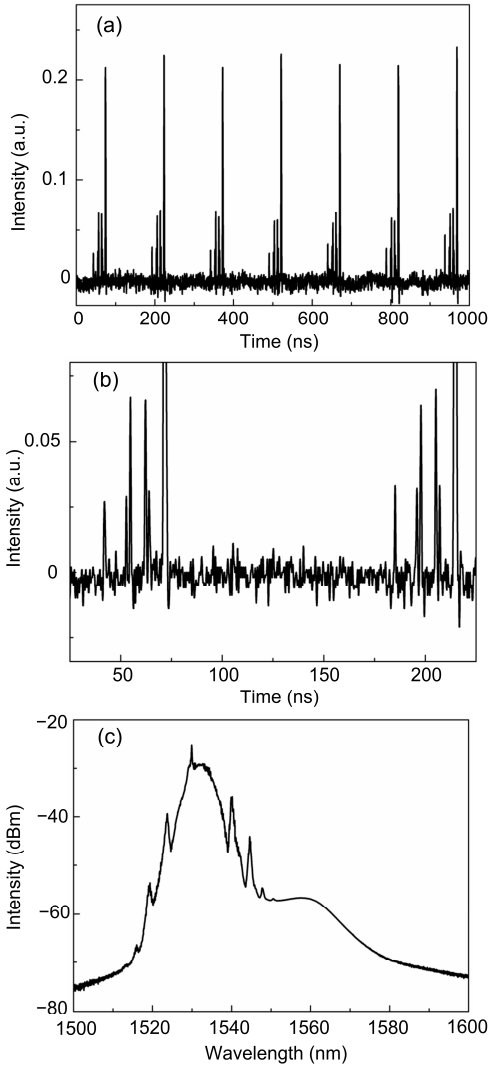

Fig. 6 Output characteristics of the soliton rains: (a) output pulse train; (b) magnification of the pulse train; (c) optical spectrum

In the temporal dynamics of soliton rains, the isolated solitons move towards the right-hand side, finally flowing into the condensed soliton part. This is similar to the process of rain droplet formation in nature. With the increase of pump power, the velocity of soliton flow increases and the amplitude of the large peak changes abruptly. When the pump power increases to 348 mW, the soliton will not flow and the pulse train becomes stable. The characteristics of the stable soliton state are shown in Fig. 7. As shown in Fig. 7a, the soliton pulse is steady and the repetition frequency is 7 MHz. The magnification of a single-pulse profile shows that the soliton pulse is square-shape (Fig. 7b), and the quasi-CW components on the output spectrum (Fig. 7c) are significantly weakened. Fig. 7d gives the measured autocorrelation trace, indicating a pulse width of 800 fs. All these results demonstrate that the operational state is no longer one of the soliton rains. From Figs. 6c and 7c, we can see that the center wavelengths are around 1530 nm, indicating the large cavity loss induced by IL and PDL of the GSA at 1550 nm.

The presence of the CW components in the spectra is a feature of soliton rains. In fact, through their interactions, CW spectral components with a large amplitude can produce severe fluctuations that can form stable solitons when the pump power increases to a certain point. The CW components can be induced by various mechanisms, such as amplified spontaneous emission and dispersive wave radiation shedding from solitons (Gordon, 1992; Soto-Crespo et al., 2003). However, the cavity dispersion, large loss, and the saturable absorption characteristics of the GSA can play important roles in the generation process of soliton rains.

4.3 Dual-wavelength mode-locking

Under a pump power of 170 mW, we obtain another mode-locked state by carefully adjusting the PC. The recorded output pulse train is presented in Fig. 8a. It can be seen that the fundamental repetition rate is about 7 MHz, which corresponds to the roundtrip time of the laser cavity. Fig. 8b shows the details of the single-pulse bunch, in which there are many small soliton pulses on the left side of the main pulse. The optical spectrum and autocorrelation trace recorded are displayed in Figs. 8c and 8d, respectively, exhibiting a measured pulse width of 610 fs and a spectrum

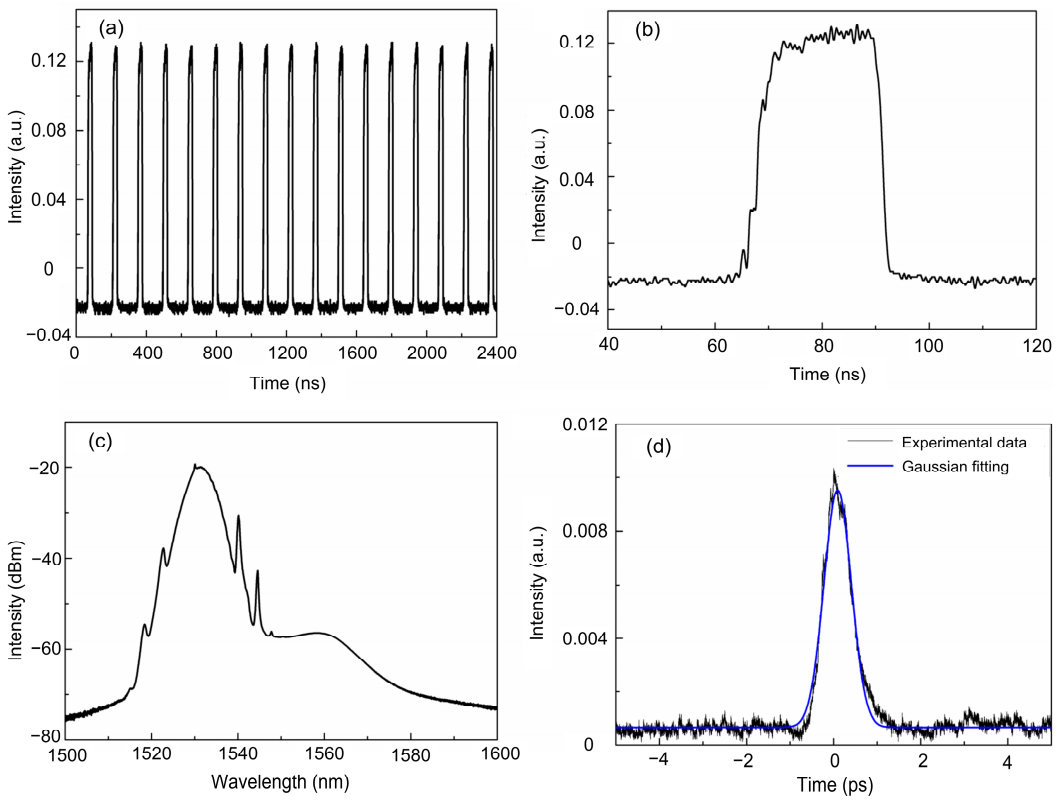

Fig. 7 Characteristics of the stable soliton state: (a) output pulse train; (b) magnification of the pulse train; (c) optical spectrum; (d) autocorrelation trace (References to color refer to the online version of this figure)

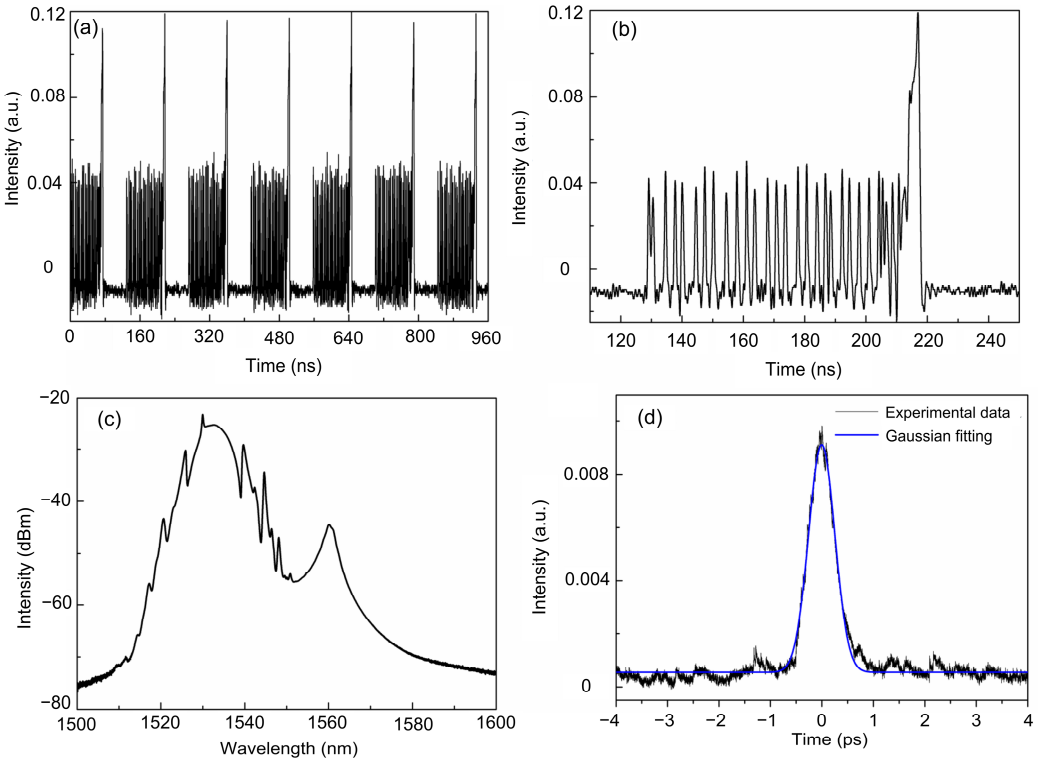

Fig. 8 Output characteristics of the soliton mode-locked state: (a) output pulse train; (b) magnification of the pulse train; (c) optical spectrum; (d) autocorrelation trace (References to color refer to the online version of this figure)

with two primary peaks locating at 1532 nm and 1560 nm. In Fig. 8c, we can see that there are many small sidelobes in the spectrum, corresponding to the small solitons in Fig. 8b. The existence of small solitons may be related to two mechanisms. On one hand, the gain relaxation dynamics means that the gain of the leading pulse is slightly higher than that of the small soliton. On the other hand, the non-uniform distribution of the background (apart from the soliton radiation) plays an important role in establishing a stable bound distance between the subsequent pulses (Chouli and Grelu, 2010). When increasing the pump power and keeping other parameters unchanged, the positions of these two peaks also change. As seen in Fig. 9a, with the increase of pump power, the relative amplitude between two peaks of the output spectrum varies, where the 1532-nm peak gradually weakens and the 1560-nm one gradually strengthens. Fig. 9b shows the pulse width under different pump powers, from which we can see that the pulse width varies considerably. The results can be related to the switching between the generation of NLP and the emission of multiple solitons (in the form of soliton rain and dual-wavelength mode-locking) with the increase of pump power.

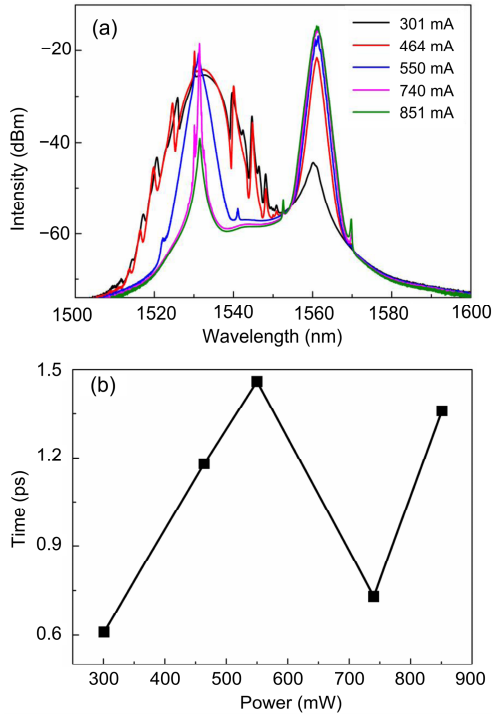

Fig. 9 Output characteristics of the soliton mode-locked state at different pump powers: (a) optical spectra; (b) pulse width of the mode-locked pulse at different pump powers (References to color refer to the online version of this figure)

5 Conclusions

We have experimentally studied the soliton operation of a mode-locked fiber laser based on the GSA, and observed various mode-locked pulse states, including NLPs, soliton rains, and the particular mode-locking at different wavelengths. Based on the experimental results on different soliton operations, we have illustrated the soliton interaction induced by the large cavity loss, the total dispersion, and the soliton-soliton attraction induced by the GSA. We believe that the research results can help better understand the formation of solitons in passively mode-locked EDFLs.

Contributors

Pinghua TANG, Mulin LUO, Ting ZHAO, and Yuliang MAO designed the research. Pinghua TANG and Mulin LUO processed the data. Pinghua TANG drafted the manuscript. Mulin LUO helped organize the manuscript. Ting ZHAO and Yuliang MAO revised and finalized the paper.

Compliance with ethics guidelines

Pinghua TANG, Mulin LUO, Ting ZHAO, and Yuliang MAO declare that they have no conflict of interest.

References

Ahmad H, Samion MZ, Sharbirin AS, et al., 2017. Dual-wavelength, passively Q-switched thulium-doped fiber laser with N-doped graphene saturable absorber. *Optik*, 149:391-397. https://doi.org/10.1016/j.ijleo.2017.09.054

Ahmed MHM, Latiff AA, Arof H, et al., 2016. Ultrafast erbium-doped fiber laser mode-locked with a black phosphorus saturable absorber. *Laser Phys Lett*, 13(9): 095104. https://doi.org/10.1088/1612-2011/13/9/095104

Bao QL, Zhang H, Wang Y, et al., 2009. Atomic-layer graphene as a saturable absorber for ultrafast pulsed lasers. *Adv Funct Mater*, 19(19):3077-3083. https://doi.org/10.1002/adfm.200901007

Chouli S, Grelu P, 2010. Soliton rains in a fiber laser: an experimental study. *Phys Rev A*, 81(6):063829. https://doi.org/10.1103/PhysRevA.81.063829

Goloborodko V, Keren S, Rosenthal A, et al., 2003. Measuring temperature profiles in high-power optical fiber components. *Appl Opt*, 42(13):2284-2288. https://doi.org/10.1364/AO.42.002284

Gordon JP, 1992. Dispersive perturbations of solitons of the nonlinear Schrödinger equation. *J Opt Soc Am B*, 9(1):91-97. https://doi.org/10.1364/JOSAB.9.000091

Jeong Y, Vazquez-Zuniga LA, Lee S, et al., 2014. On the formation of noise-like pulses in fiber ring cavity configurations. *Opt Fiber Technol*, 20(6):575-592. https://doi.org/10.1016/j.yofte.2014.07.004

Kasim N, Latiff AA, Rusdi MFM, et al., 2018. Short-pulsed Q-switched Thulium doped fiber laser with graphene oxide as a saturable absorber. *Optik*, 168:462-466. https://doi.org/10.1016/j.ijleo.2018.04.117

Kobtsev S, Kukarin S, Smirnov S, et al., 2014. Cascaded SRS of single- and double-scale fiber laser pulses in long extra-cavity fiber. *Opt Expr*, 22(17):20770-20775. https://doi.org/10.1364/OE.22.020770

Li D, Xue H, Qi M, et al., 2017. Graphene actively Q-switched lasers. *2D Mater*, 4(2):025095. https://doi.org/10.1088/2053-1583/aa6e6b

Li J, Zhang ZL, Du L, et al., 2019. Highly stable femtosecond pulse generation from a MXene $Ti_3C_2T_x$ (T=F, O, or OH) mode-locked fiber laser. *Photon Res*, 7(3):260-264. https://doi.org/10.1364/PRJ.7.000260

Liu J, Chen Y, Tang PH, et al., 2015. Generation and evolution of mode-locked noise-like square-wave pulses in a large-anomalous-dispersion Er-doped ring fiber laser. *Opt Expr*, 23(5):6418-6427. https://doi.org/10.1364/OE.23.006418

Liu J, Wu JD, Chen HL, et al., 2021. Short-pulsed Raman fiber laser and its dynamics. *Sci China Phys Mech Astron*, 64(1):214201. https://doi.org/10.1007/s11433-020-1591-2

Luo AP, Luo ZC, Liu H, et al., 2015. Noise-like pulse trapping in a figure-eight fiber laser. *Opt Expr*, 23(8):10421-10427. https://doi.org/10.1364/OE.23.010421

Luo ZC, Liu M, Liu H, et al., 2013. 2 GHz passively harmonic mode-locked fiber laser by a microfiber-based topological insulator saturable absorber. *Opt Lett*, 38(24):5212-5215. https://doi.org/10.1364/OL.38.005212

Ma CY, Huang WC, Wang YZ, et al., 2020. MXene saturable absorber enabled hybrid mode-locking technology: a new routine of advancing femtosecond fiber lasers performance. *Nanophotonics*, 9(8):2451-2458. https://doi.org/10.1515/nanoph-2019-0527

Ma R, Rao YJ, Zhang WL, et al., 2019. Multimode random fiber laser for speckle-free imaging. *IEEE J Sel Top Quant Electron*, 25(1):0900106. https://doi.org/10.1109/JSTQE.2018.2833472

Martinez A, Fuse K, Xu B, et al., 2010. Optical deposition of graphene and carbon nanotubes in a fiber ferrule for passive mode-locked lasing. *Opt Expr*, 18(22):23054-23061. https://doi.org/10.1364/OE.18.023054

Meng YC, Zhang SM, Li XL, et al., 2012. Multiple-soliton dynamic patterns in a graphene mode-locked fiber laser. *Opt Expr*, 20(6):6685-6692. https://doi.org/10.1364/OE.20.006685

Nelson LE, Jones DJ, Tamura K, et al., 1997. Ultrashort-pulse fiber ring lasers. *Appl Phys B*, 65(2):277-294. https://doi.org/10.1007/s003400050273

Ng EK, Lau KY, Lee HK, et al., 2020. Saturable absorber incorporating graphene oxide polymer composite through dip coating for mode-locked fiber laser. *Opt Mater*, 100:109619. https://doi.org/10.1016/j.optmat.2019.109619

Niang A, Amrani F, Salhi M, et al., 2014. Rains of solitons in a figure-of-eight passively mode-locked fiber laser. *Appl Phys B*, 116(3):771-775. https://doi.org/10.1007/s00340-014-5760-y

Ning QY, Liu H, Zheng XW, et al., 2014. Vector nature of multi-soliton patterns in a passively mode-locked figure-eight fiber laser. *Opt Expr*, 22(10):11900-11911. https://doi.org/10.1364/OE.22.011900

Ozgören K, Oktem B, Yilmaz S, et al., 2011. 83 W, 3.1 MHz, square-shaped, 1 ns-pulsed all-fiber-integrated laser for micromachining. *Opt Expr*, 19(18):17647-17652. https://doi.org/10.1364/OE.19.017647

Pawliszewska M, Martynkien T, Przewłoka A, et al., 2018. Dispersion-managed Ho-doped fiber laser mode-locked with a graphene saturable absorber. *Opt Lett*, 43(1):38-41. https://doi.org/10.1364/OL.43.000038

Popa D, Sun Z, Hasan T, et al., 2011. Graphene Q-switched, tunable fiber laser. *Appl Phys Lett*, 98(7):073106. https://doi.org/10.1063/1.3552684

Popa D, Jiang Z, Bonacchini GE, et al., 2017. A stable, power scaling, graphene-mode-locked all-fiber oscillator. *Appl Phys Lett*, 110(24):243102. https://doi.org/10.1063/1.4985293

Sheng QW, Feng M, Xin W, et al., 2013. Actively manipulation of operation states in passively pulsed fiber lasers by using graphene saturable absorber on microfiber. *Opt Expr*, 21(12):14859-14866. https://doi.org/10.1364/OE.21.014859

Shi Z, Cao R, Khan K, et al., 2020. Two-dimensional tellurium: progress, challenges, and prospects. *Nano-Micro Lett*, 12:99. https://doi.org/10.1007/s40820-020-00427-z

Smirnov SV, Kobtsev SM, Kukarin SV, 2014. Efficiency of non-linear frequency conversion of double-scale pico-femtosecond pulses of passively mode-locked fiber laser. *Opt Expr*, 22(1):1058-1064. https://doi.org/10.1364/OE.22.001058

Song YF, Li L, Zhang H, et al., 2013. Vector multi-soliton operation and interaction in a graphene mode-locked fiber laser. *Opt Expr*, 21(8):10010-10018. https://doi.org/10.1364/OE.21.010010

Song YF, Chen S, Zhang Q, et al., 2016. Vector soliton fiber laser passively mode locked by few layer black phosphorus-based optical saturable absorber. *Opt Expr*, 24(23):25933-25942. https://doi.org/10.1364/OE.24.025933

Soto-Crespo JM, Akhmediev N, Grelu P, et al., 2003. Quantized separations of phase-locked soliton pairs in fiber lasers. *Opt Lett*, 28(19):1757-1759. https://doi.org/10.1364/OL.28.001757

Tang PH, Qin ZP, Liu J, et al., 2015. Watt-level passively mode-locked Er^{3+}-doped ZBLAN fiber laser at 2.8 μm. *Opt Lett*, 40(21):4855-4858. https://doi.org/10.1364/OL.40.004855

Tang PH, Wu M, Wang QK, et al., 2016. 2.8 μm pulsed Er^{3+}: ZBLAN fiber laser modulated by topological insulator.

IEEE Photon Technol Lett, 28(14):1573-1576. https://doi.org/10.1109/LPT.2016.2555989

Tang YL, Yu XC, Li XH, et al., 2014. High-power thulium fiber laser *Q* switched with single-layer graphene. *Opt Lett*, 39(3):614-617. https://doi.org/10.1364/OL.39.000614

Wang ZH, Wang Z, Liu YG, et al., 2016. Q-switched-like soliton bunches and noise-like pulses generation in a partially mode-locked fiber laser. *Opt Expr*, 24(13): 14709-14716. https://doi.org/10.1364/OE.24.014709

Woodward RI, Howe RCT, Hu G, et al., 2015. Few-layer MoS_2 saturable absorbers for short-pulse laser technology: current status and future perspectives [Invited]. *Photon Res*, 3(2):A30-A42. https://doi.org/10.1364/PRJ.3.000A30

Yun L, 2017. Switchable dual-wavelength conventional soliton delivered from a graphene-mode-locked fiber laser. *Optik*, 145:549-554. https://doi.org/10.1016/j.ijleo.2017.08.024

Zaytsev A, Lin CH, You YJ, et al., 2013. Supercontinuum generation by noise-like pulses transmitted through normally dispersive standard single-mode fibers. *Opt Expr*, 21(13):16056-16062. https://doi.org/10.1364/OE.21.016056

Zeng C, Cui YD, Guo J, 2015. Observation of dual-wavelength solitons and bound states in a nanotube/microfiber mode-locking fiber laser. *Opt Commun*, 347:44-49. https://doi.org/10.1016/j.optcom.2015.02.054

Zhang H, Tang DY, Zhao LM, et al., 2009. Large energy mode locking of an erbium-doped fiber laser with atomic layer graphene. *Opt Expr*, 17(20):17630-17635. https://doi.org/10.1364/OE.17.017630

Zhang H, Lu SB, Zheng J, et al., 2014. Molybdenum disulfide (MoS_2) as a broadband saturable absorber for ultra-fast photonics. *Opt Expr*, 22(6):7249-7260. https://doi.org/10.1364/OE.22.007249

Zhao CJ, Zhang H, Qi X, et al., 2012. Ultra-short pulse generation by a topological insulator based saturable absorber. *Appl Phys Lett*, 101(21):211106. https://doi.org/10.1063/1.4767919